PERGAMON

International Journal of Heat and Mass Transfer 44 (2001) 3787–3798

International Journal of HEAT and MASS TRANSFER

www.elsevier.com/locate/ijhmt

Material response to thermal loading due to short pulse laser heating

B.S. Yilbas *, A.F.M. Arif

Department of Mechanical Engineering, King Fahd University of Petroleum and Minerals, P.O. Box 1913, Dhahran 31261, Saudi Arabia

Received 2 May 2000; received in revised form 10 January 2001

Abstract

The laser-induced thermal stresses are important during heating of substrate surfaces, since stress levels above the yield stress of the substrate material occur. In this case, the plastic deformation and/or material defects occur in the irradiated region. In the present study, laser short pulse heating of gold is considered. The electron kinetic theory approach is employed to model the heating process. This approach accounts for the non-equilibrium energy transport in the surface vicinity of the substrate material. The thermal analysis and temperature predictions from an electron kinetic theory approach were presented in a previous study. Therefore, the results of thermo-elastic analysis due to the temperature field predicted in the previous study are given here. The elastic stresses developed in the substrate material due to the temperature field are modelled, and the temporal and spatial variations of the stress field and von Mises stresses are computed. It is found that the stress field in the substrate material does not follow the temperature field. A stress level on the order of 10^9 Pa occurs in the surface vicinity.

1. Introduction

Laser short pulse heating of metallic substrates initiates non-equilibrium energy transport in the surface vicinity of the substrate material. In this case, the use of the Fourier heating model overestimates the temperature rise in the surface vicinity [1]. This is because the high order terms, which are neglected in the Fourier heating model, become important in the energy transport process [2]. Moreover, diffusion in metals takes place due to subsequent collisions between excited electrons and lattice site atoms. Consequently, the temperature distribution in the substrate material depends on the electron energy distribution and the number of collisions that takes place in the region considered. Harrington [3] showed that electrons within a five electron mean free path contribute 98.5% of the total energy transported provided that $\partial T/\partial x$ was constant over at least this distance. Consequently, when examining the energy transport in metals due to laser short pulse heating, a microscopic level consideration employing electron lattice site atom collision is necessary.

Considerable research studies have been carried out to explore the temperature field in the substrate material due to short pulse laser heating. The non-equilibrium heating of a tungsten surface due to femtosecond laser irradiation was investigated by Fujimoto et al. [4]. They used the two-equation model to describe the electron–phonon coupling process and predicted the electron temperature. They indicated that the relaxation time for electron–phonon energy coupling is on the order of hundred femtoseconds. The temporal behavior of non-equilibrium electron and lattice temperatures in copper due to laser short pulse heating was examined by Elsayed-Ali et al. [5]. They monitored the thermal modulation of the transmissivity of thin copper films and predicted the electron temperatures using the two-equation model. They indicated that a few thousands degrees of difference between electron and lattice temperatures occur in the early interaction time (~1 ps). Qiu and Tien [6] studied microscopic energy deposition and transport processes during laser short pulse heating of multi-layer metals. The predictions showed that multi-layer metals presented very different thermal responses from a single layer metal during the heating process. The

* Corresponding author. Tel.: +966-3-860-2540; fax: +966-3-860-2949.

E-mail address: bsyilbas@kfupm.edu.sa (B.S. Yilbas).

0017-9310/01/$ - see front matter
PII: S0017-9310(01)00026-6

Nomenclature

a Gaussian parameter (m)
C_p specific heat capacity (J/m^{3}K)
E modulus of elasticity (Pa)
f fraction of electron excess energy transferring from the lattice site during a single collision
G shear modulus (Pa)
h enthalpy (J/Kg)
I_0 peak power intensity (W/m^2)
k thermal conductivity (W/mK)
N number of electrons
r_f surface reflectivity
s distance along the x-axis for electron movement (m)
t time (s)
$T(x,y,z,t)$ temperature (K)
x distance along the x-axis (m)
y distance along the y-axis (m)
z distance along the z-axis (m)
D elasticity matrix
ΔT temperature rise at a point (x,y,z) at time $= t$ with respect to that at $t = 0$
T_{ref} reference temperature at $t = 0$
$\{f^B\}$ the applied body force
$\{P\}$ the applied pressure vector
$\{\overline{F}\}$ concentrated nodal forces to the element
$\{\delta U\}$ virtual displacement
$\{\delta U_s\}$ virtual displacement on the boundary where pressure is prescribed
$\{\delta\overline{U}\}$ virtual displacement of boundary nodes where concentrated load is prescribed
$[B]$ strain displacement gradient matrix
$\{\overline{U}\}$ nodal displacement vector
$[N]$ matrix of shape (or interpolation) functions
$[K_e] = \int_\forall [B]^T[D][B]\,d\forall$ element stiffness matrix
$\{F^{th}\} = \int_\forall [B]^T[D][\epsilon^{th}]\,d\forall$ element thermal load vector
$\{F\}^b = \int_\forall [N]^T[f^B]\,d\forall$ element applied body force vector
$\{F\}^s = \int_{\eth\eth} [N_n]^T[P]\,d\eth$ element pressure vector
$[N_n]$ shape functions for normal displacement at the boundary surface

Greek symbols

Δ increment
θ electron temperature (K)
η distance along the y-axis for electron movement (m)
σ stress vector (MPa)
σ_p principal stress (MPa)
ζ distance along the z-axis for electron movement (m)
$\{\epsilon\}$ total strain vector
$\{\epsilon^{th}\}$ thermal strain vector
ϵ' equivalent strain
α thermal diffusivity (m^2/s)
α_e coefficient of thermal expansion in strain (1/K)
α_σ coefficient of thermal expansion in stress (J/m^3 K)
υ Poisson's ratio
δ absorption coefficient (1/m)
λ mean free path (m)
ρ density (kg/m^3)

two-equation model for laser short pulse heating of metal surfaces was presented by Phinney and Tien [7]. They identified the regimes of predominantly electronic and thermal desorption. A simplified approach was introduced by Al-Nimr and Arpaci [8] to describe the thermal behavior of a tin metal film exposed to picosecond thermal pulses. The approach eliminated the coupling between the energy equations and simplified the governing differential equations. Tzou [9] introduced a unified field approach for heat conduction for micro-to-micro scales. He indicated that the universal form of the energy equation facilitated identification of the physical parameters governing the transition from diffusion to electron–phonon interaction. Yilbas [10] introduced the electron kinetic theory approach to describe the non-equilibrium energy transport due to laser short pulse heating of metallic surfaces. He indicated that the predictions of electron kinetic theory approach the Fourier theory results as the duration of heating extends to nanoseconds. He further argued that the electron temperature attained higher values than the lattice site temperatures in the surface vicinity of the substrate material for sub-nanosecond heating pulses [1].

When the substrate material is irradiated by a high intensity and short laser pulse, an anomalous temperature rise occurs in the surface vicinity. This results in thermal expansion of the substrate material, which in turn develops thermal stresses in the irradiated region. The magnitude of the thermal stresses, in some cases, exceeds the yield stress of the substrate material, which in turn results in plastic deformation in the heated region. A considerable number of research studies have been carried out to identify the stress field in the irradiated region. Most of the studies, however, were limited to long pulses or continuous laser heating processes.

Modest [11] studied the elastic and viscoplastic responses of ceramics during laser drilling. He showed that the substrate material softened near the ablation front. The plane stress model was introduced by Li and Sheng [12] for fracture initiation during laser cutting of ceramics. A fracture initiation was determined based on the maximum tensile and compressive stresses. They indicated that low cutting speed resulted in a wider kerf and a low stress levels. Dain et al. [13] investigated the stress development along the weld direction. The analytical expressions for the mismatch and the stress tensor were obtained for the thermo-elastic infinite plate in terms of a convolution integral depending on the general heat sources. They indicated that their findings for the distortion gap was in agreement with the experimental findings. Elperin and Rudin [14] developed an analytical model for a two-dimensional thermo-elastic response of multilayer coating due to laser irradiation. They determined non-stationary temperature, strain, and stress distributions in a multilayer assembly. They indicated that the temperature rise across the irradiated surface resulted in stress levels which caused an irreversible damage to the coatings. Yilbas et al. [15] investigated the laser induced thermal stresses on steel surfaces. They indicated that the excessive stress levels occur in the surface vicinity of the substrate.

In the light of the above arguments, the present study is conducted as an extension of the previous work [16]. The thermal stresses due to the temperature field resulting from a short pulse laser heating is modeled. The resulting stresses in the axial and transverse directions are computed. The temporal and spatial variations of von Mises stress are obtained in the irradiated region.

2. Energy transport model

The electron–phonon collision mechanism through which the energy exchange between the electrons and lattice site atoms occurs is considered in the electron kinetic theory approach. The mathematical arrangements of the governing equation are given in [17,18]. The final form of the energy equation resulting from the kinetic theory is presented here. Therefore, the resulting equation pertinent to the laser heating pulse is

$$\begin{aligned}\rho C_{\mathrm{p}}\frac{\partial T(x,y,z,t)}{\partial t} = {} & \int_{-\infty}^{\infty}\frac{fk}{\lambda^3}\exp\left(-\frac{|x-s|}{\lambda}\right)\\ & \times[\theta(s,y,z,t)-T(x,y,z)]\,\mathrm{d}s\\ & +\int_{-\infty}^{\infty}\frac{fk}{\lambda^3}\exp\left(-\frac{|y-\eta|}{\lambda}\right)\\ & \times[\theta(x,\eta,z,t)-T(x,y,z)]\,\mathrm{d}\eta\\ & +\int_{-\infty}^{\infty}\frac{fk}{\lambda^3}\exp\left(-\frac{|y-\varsigma|}{\lambda}\right)\\ & \times[\theta(x,y,\varsigma,t)-T(x,y,z)]\,\mathrm{d}\varsigma\\ & +\int_{-\infty}^{\infty}\frac{I_{\mathrm{surf}}}{\lambda^2}\frac{fN_{sx}}{N_{sx}+N_{xs}}\\ & \times\exp\left(-\frac{|x-s|}{\lambda}\right)\int_{x}^{s}f'(\varphi)\,\mathrm{d}\varphi\,\mathrm{d}s \end{aligned}\tag{1}$$

and

$$\begin{aligned}&\int_{-\infty}^{\infty}\frac{k}{\lambda^3}\exp\left(-\frac{|x-s|}{\lambda}\right)[\theta(s,y,z,t)-fT(x,y,z,t)]\,\mathrm{d}s\\ &+\int_{-\infty}^{\infty}\frac{k}{\lambda^3}\exp\left(-\frac{|x-\eta|}{\lambda}\right)[\theta(x,\eta,z,t)-fT(x,y,z,t)]\,\mathrm{d}\eta\\ &+\int_{-\infty}^{\infty}\frac{k}{\lambda^3}\exp\left(-\frac{|x-\varsigma|}{\lambda}\right)[\theta(x,y,\varsigma,t)-fT(x,y,z,t)]\,\mathrm{d}\varsigma\\ &=\int_{-\infty}^{\infty}\frac{k}{\lambda^3}\exp\left(-\frac{|x-s|}{\lambda}\right)(1-f)\theta(s,y,z,t)\,\mathrm{d}s\\ &\quad+\int_{-\infty}^{\infty}\frac{k}{\lambda^3}\exp\left(-\frac{|x-\eta|}{\lambda}\right)(1-f)\theta(x,\eta,z,t)\,\mathrm{d}\eta\\ &\quad+\int_{-\infty}^{\infty}\frac{k}{\lambda^3}\exp\left(-\frac{|x-\varsigma|}{\lambda}\right)(1-f)\theta(x,y,\varsigma,t)\,\mathrm{d}\varsigma\\ &\quad+\int_{-\infty}^{\infty}(1-f)\frac{N_{sx}}{N_{sx}+N_{xs}}\\ &\quad\times\exp\left(-\frac{|x-s|}{\lambda}\right)\int_{x}^{s}f'(\varphi)\,\mathrm{d}\varphi\,\mathrm{d}s. \end{aligned}\tag{2}$$

Eqs. (1) and (2) are the equations of interest for laser machining. The method of solution to be used in the following analysis is the transformation of the simultaneous differential–integral equations (1) and (2) using the Fourier integral transformation, with respect to x, y, and z. The resultant ordinary differential equations may then be handled much more conveniently. The three-dimensional analysis of Fourier transformation, which is considered in the present study, is similar to that carried out in the previous study [16]; therefore, only the resulting equation is given below, i.e.,

$$\begin{aligned}&\left[1-\frac{\lambda^2}{f}\left(\frac{\partial^2}{\partial x^2}+\frac{\partial^2}{\partial y^2}+\frac{\partial^2}{\partial z^2}\right)\right]\rho C_{\mathrm{p}}\frac{\partial T}{\partial t}\\ &\quad=k\left(\frac{\partial^2 T}{\mathrm{d}x^2}+\frac{\partial^2 T}{\mathrm{d}y^2}+\frac{\partial^2 T}{\mathrm{d}z^2}\right)+I_{\mathrm{surf}}\delta\exp(-\delta|x|)\end{aligned}\tag{3}$$

I_{surf} is the power intensity distribution at the surface, which is

$$I_{\mathrm{surf}}=\frac{I_0(1-r_f)}{\sqrt{\pi}a}\exp\left(-\frac{y^2+z^2}{a^2}\right),$$

where a is the Gaussian parameter, r_{f} is the surface reflectivity, and I_0 is the power intensity. The lattice site temperature can be obtained from Eq. (3), which is the differential form of Eqs. (1) and (2). Moreover, if the term $(\lambda^2/f)(\partial^2/\partial x^2+\partial^2/\partial x^2+\partial^2/\partial x^2)(\rho C_{\mathrm{p}}\partial T/\partial t)$ is neglected for all f values, Eq. (3) becomes

$$\rho C_{\mathrm{p}} \frac{\partial T}{\partial t} = k\left(\frac{\partial^2 T}{\mathrm{d}x^2} + \frac{\partial^2 T}{\mathrm{d}x^2} + \frac{\partial^2 T}{\mathrm{d}x^2}\right) + I_{\mathrm{surf}}\delta \exp(-\delta|x|)$$

which is exactly the same as a Fourier heat conduction equation as described in the previous study [16]. Therefore, the equations derived from the electron kinetic theory approach for the heat conduction process are more general than the Fourier equation.

In order to account for the thermomechanical effect during the heating process, the energy transport equation (Eq. (3)) should be modified. For a deformable solid body, the specific enthalpy can be written as [19]

$$h \equiv h(T, e),$$

where e is the strain. The enthalpy can be written as

$$\rho\, \mathrm{d}h = \rho\left(\frac{\partial h}{\partial T}\right)_{\mathrm{e}} \mathrm{d}T + \rho\left(\frac{\partial h}{\partial e}\right)_{T} \mathrm{d}e.$$

It was shown that [19]

$$\rho\left(\frac{\partial h}{\partial e}\right)_{T} \cong \left(\frac{\partial C_{\mathrm{v}}}{\partial T}\right)_{T_0} T_0,$$

where C_{v} is the volumetric specific heat and T_0 is the reference temperature. However,

$$-\nabla \cdot q = \rho\, \mathrm{d}h$$

or

$$-\nabla \cdot q = C_{\mathrm{p}} \frac{\partial T}{\partial t} + \alpha_\sigma T_0 \left(\frac{\partial e}{\partial t}\right), \tag{4}$$

where α_σ is related to the coefficient of thermal expansion and it is

$$\alpha_\sigma \equiv \left(\frac{\partial C_{\mathrm{v}}}{\partial T}\right).$$

Rearrangement of Eq. (4) yields

$$-\nabla \cdot q = C_{\mathrm{p}} \frac{\partial T}{\partial t}\left[1 + \frac{\alpha_\sigma T_0 (\partial e/\partial t)}{C_{\mathrm{p}}\, \mathrm{d}T}\right]$$

or

$$-\nabla \cdot q = C_{\mathrm{p}} \frac{\partial T}{\partial t}\left[1 + \eta\left(\frac{\partial e/\partial t}{\alpha_{\mathrm{e}} \mathrm{d}T}\right)\right],$$

where η ($\eta = (3G\alpha_{\mathrm{e}}^2 T_0)/C_{\mathrm{p}}$, $\alpha_{\mathrm{e}} = \alpha_\sigma/3G$, and $G = E/3(1-2\upsilon)$) is the thermomechanical coupling factor, which is shown to be small for most metals at room temperature [19].

The stress components can be written as

$$\begin{aligned} \sigma_x &= Ee_x - E\alpha_{\mathrm{e}} T, \\ \sigma_y &= Ee_y - E\alpha_{\mathrm{e}} T, \\ \sigma_z &= Ee_z - E\alpha_{\mathrm{e}} T \end{aligned} \tag{5}$$

with

$$\begin{aligned} e_x &= \frac{\partial U}{\partial x}, \\ e_y &= \frac{\partial U}{\partial y}, \\ e_z &= \frac{\partial U}{\partial z}, \end{aligned} \tag{6}$$

where U is the thermal displacement. In the stress field the equilibrium condition yields [20]

$$\nabla \cdot \sigma = \rho \frac{\partial^2 U}{\partial t^2}. \tag{7}$$

Therefore,

$$\nabla^2 U - \alpha_{\mathrm{e}}(\nabla \cdot T) = \frac{\rho}{E}\frac{\partial^2 U}{\partial t^2}. \tag{8}$$

Using Eqs. (5)–(7), and combining Eqs. (4) and (8), it yields

$$-\nabla \cdot q = C_{\mathrm{p}} \frac{\partial T}{\partial t} + \left(\frac{C_{\mathrm{p}}\eta}{\alpha_{\mathrm{e}}}\right)\frac{\partial}{\partial t}(\nabla \cdot U). \tag{9}$$

The equation describing the energy transport due to electron–phonon interactions (Eq. (3)) can be written as

$$\begin{aligned} -\nabla \cdot q = k(\nabla^2, T) + \frac{C_{\mathrm{p}}\lambda^2}{f}\frac{\partial}{\partial t}(\nabla^2 \cdot T) \\ + I_{\mathrm{surf}}\delta \exp(-\delta|x|). \end{aligned} \tag{10}$$

Combining Eqs. (9) and (10), it yields

$$\begin{aligned} \frac{\partial T}{\partial t} = \alpha\nabla^2 \cdot T + \frac{\lambda^2}{f}\frac{\partial}{\partial t}(\nabla^2 \cdot T) - \left(\frac{\eta}{\alpha_{\mathrm{e}}}\right)\frac{\partial}{\partial t}(\nabla \cdot U) \\ + I_{\mathrm{surf}}\frac{\delta}{C_{\mathrm{p}}} \exp(-\delta|x|). \end{aligned} \tag{11}$$

Eq. (10) is the general energy transport equation, which includes the thermomechical effect.

Initial condition is: at $t = 0 \rightarrow T = 0$ and $U = 0$.

Boundary conditions are: Since the laser pulse length and heating duration are short, there is no convective nor radiative losses are considered from the surface

$$\text{At } t \neq 0 \text{ and at the surface } \left.\frac{\partial T}{\partial x}\right|_{\mathrm{surface}} = 0,$$

$$\text{At } t \neq 0 \text{ and } x = y = z = \infty \rightarrow T = 0 \text{ and } U = 0.$$

3. Thermal stress model

During laser material processing, the heating is localized and, therefore, a very large temperature variation occurs over a small region. Owing to this temperature gradient, large thermal stresses are generated in the substrate, which can lead to the defects in the material such as the formation of cracks and fractures in the material. The stress is related to strains by

$$\{\sigma\} = [D]\{\epsilon^{e}\}, \tag{12}$$

where $\{\sigma\}$ is the stress vector, and $[D]$ is the elasticity matrix.

$$\{\epsilon^{e}\} = \{\epsilon\} - \{\epsilon^{th}\},$$

where $\{\epsilon\}$ is the total strain vector and $\{\epsilon^{th}\}$ is the thermal strain vector.

Eq. (12) may also be written as

$$\{\epsilon\} = [D]^{-1}\{\sigma\} + \{\epsilon^{th}\}. \tag{13}$$

Since the present case is axially symmetric, and the material is assumed to be isotropic, the above stress–strain relations can be written in Cartesian coordinates as

$$\begin{aligned}
\epsilon_{xx} &= \frac{1}{E}\left[\sigma_{xx} - \upsilon\left(\sigma_{yy} + \sigma_{zz}\right)\right] + \alpha_{e}\Delta T,\\
\epsilon_{yy} &= \frac{1}{E}\left[\sigma_{yy} - \upsilon(\sigma_{xx} + \sigma_{zz})\right] + \alpha_{e}\Delta T,\\
\epsilon_{zz} &= \frac{1}{E}\left[\sigma_{zz} - \upsilon\left(\sigma_{xx} + \sigma_{yy}\right)\right] + \alpha_{e}\Delta T,\\
\epsilon_{yx} &= \frac{1+\upsilon}{E}\sigma_{xy}, \quad \epsilon_{xz} = \frac{1+\upsilon}{E}\sigma_{xz}, \quad \epsilon_{yz} = \frac{1+\upsilon}{E}\sigma_{yz},
\end{aligned} \tag{14}$$

where E, υ, and α_{e} are the modulus of elasticity, Poisson's ratio, and coefficient of thermal expansion, respectively. ΔT represents the temperature rise at a point (x, y, z) at time $= t$ with respect to that at $t = 0$ corresponding to a stress free condition. A typical component of thermal strain from Eq. (14) is

$$\epsilon^{th} = \alpha_{e}\Delta T = \alpha_{e}(T - T_{ref}), \tag{15}$$

where T_{ref} is the reference temperature at $t = 0$.

When α_{e} is a function of temperature, then Eq. (15) becomes

$$\epsilon^{th} = \int_{T_{ref}}^{T} \alpha_{e}(T)\,\mathrm{d}T. \tag{16}$$

The present study uses a mean or weighted-average value of α, such that

$$\epsilon^{th} = \overline{\alpha_{e}}(T)(T - T_{ref}), \tag{17}$$

where $\overline{\alpha}(T)$ is the mean value of coefficient of thermal expansion and is given by

$$\overline{\alpha_{e}}(T) = \frac{\int_{T_{ref}}^{T} \alpha_{e}(T)\,\mathrm{d}T}{T - T_{ref}}. \tag{18}$$

The principal stresses $(\sigma_1, \sigma_2, \sigma_3)$ are calculated from the stress components by the cubic equation

$$\begin{vmatrix}
\sigma_{xx} - \sigma_{p} & \sigma_{xy} & \sigma_{xz}\\
\sigma_{xy} & \sigma_{yy} - \sigma_{p} & \sigma_{yz}\\
\sigma_{xz} & \sigma_{yz} & \sigma_{zz} - \sigma_{p}
\end{vmatrix} = 0,$$

where σ_{p} is the principal stress.

The von Mises or equivalent stress, σ', is computed as

$$\sigma' = \sqrt{\frac{1}{2}\left[(\sigma_1 - \sigma_2)^2 + (\sigma_2 - \sigma_3)^2 + (\sigma_3 - \sigma_1)^2\right]}.$$

The equivalent stress is related to the equivalent strain through

$$\sigma' = E\epsilon',$$

where ϵ' is equivalent strain.

Boundary conditions for stresses: Since there is no surface tractions are involved in the problem under consideration the corresponding boundary and initial conditions are introduced:

At $t = 0 \rightarrow \sigma = 0$

and

At $t \neq 0$ and at the surface $\rightarrow \sigma_{surface} = 0$

$t \neq 0$ and $x = y = z = \infty \rightarrow \sigma = 0$.

3.1. Calculation procedure

Since the energy transport equation and equation for thermal stresses are coupled through displacement and temperature, the iterative procedure is introduced when solving both equations simultaneously. However, if the thermal displacement field is known, then, the temperature field can be easily determined from the energy transport equation (Eq. (10)). In this case, let a tentatively calculated temperature on a guess displacement U^{*} is denoted by T^{*}. Let the correct displacement is obtained from $U = U^{*} + U'$ and the corresponding correction in temperature is $T = T^{*} + T'$. To proceed the iterative procedure, the following steps are considered:

- Guess the displacement (U^{*});
- solve the energy transport equation to obtain the temperature (T^{*});
- solve the equation for the displacement using T^{*};
- treat the new computed displacement as a new guess displacement (U^{*});
- repeat the iterative procedure unless $U'/U < 10^{-3}$.

The numerical method employed to solve the energy transport equation (Eq. (10)) uses a finite difference scheme, which is well established in the literature [21]. In order to obtain accurate results, the convergency criteria should be met. The stability criteria for the numerical scheme is given as follows:

Table 1
Properties of substrates used in the computation

δ (1/m)	α (m^2/s)	C_l (J/km^3)	λ (m)	E (GPa)	G (GPa)	v	$\alpha_e \times 10^{-6}$ (1/K)
6.16×10^7	1.26×10^{-4}	2.5×10^6	10^{-9}	77	36.96	0.44	14

$$
\begin{aligned}
1 \geqslant\ & ABS\begin{bmatrix} \frac{f\rho C_p}{\Delta t} + 2\lambda^2\rho C_p\left[\frac{1}{\Delta t(\Delta x)^2}+\frac{1}{\Delta t(\Delta y)^2}+\frac{1}{\Delta t(\Delta z)^2}\right] \\ -2kf\left[\frac{1}{(\Delta x)^2}+\frac{1}{(\Delta y)^2}+\frac{1}{(\Delta z)^2}\right] \end{bmatrix} \\
& + ABS\left\{\frac{kf}{(\Delta x)^2}-\frac{2\lambda^2\rho C_p}{\Delta t(\Delta x)^2}\right\} + ABS\left\{\frac{kf}{(\Delta y)^2}-\frac{2\lambda^2\rho C_p}{\Delta t(\Delta y)^2}\right\} \\
& + ABS\left\{\frac{kf}{(\Delta z)^2}-\frac{2\lambda^2\rho C_p}{\Delta t(\Delta z)^2}\right\} \\
& + ABS\left\{\frac{2\lambda^2\rho C_p}{\Delta t(\Delta x)^2}+\frac{2\lambda^2\rho C_p}{\Delta t(\Delta y)^2}+\frac{2\lambda^2\rho C_p}{\Delta t(\Delta z)^2}\right\} \\
& - ABS\left\{\frac{f\rho C_p}{\Delta t}+2\lambda^2\rho C_p \right. \\
& \left. \times\left[\frac{1}{\Delta t(\Delta x)^2}+\frac{1}{\Delta t(\Delta y)^2}+\frac{1}{\Delta t(\Delta z)^2}\right]\right\},
\end{aligned}
$$

where Δx, Δy, and Δz are spatial increments in x, y, and z axes while Δt is the time increment.

To develop a finite element procedure for stress computation, the standard displacement-based finite element method is used. The basis of this approach is the principle of virtual work, which states that the equilibrium of any body under loading requires that for any compatible small virtual displacements (which are zero at the boundary points and surfaces and corresponding to the components of displacements that are prescribed at those points and surfaces) imposed on the body in its state of equilibrium, the total internal virtual work or strain energy (δU) is equal to the total external work due to the applied thermally induced loads (δV), i.e., $\delta U = \delta V$. For the static analysis of problems having linear geometry and thermo-elastic material behavior, one can derive the following equation using standard procedure [22]

$$
\begin{aligned}
& \int_\forall \left(\{\delta\epsilon\}^T[D]\{\epsilon\} - \{\delta\epsilon\}^T[D]\{\epsilon^{th}\}\right) d\forall \\
& = \int_\forall \{\delta U\}^T\{f^B\}\, d\forall + \int_\eth \{\delta U_s\}^T\{P\}\, d\eth \\
& \quad + \sum \{\delta\overline{U}\}^T\{\overline{F}\}, \qquad (19)
\end{aligned}
$$

where $\{f^B\}$ is the applied body force; $\{P\}$ is the applied pressure vector; $\{\overline{F}\}$ is the concentrated nodal forces to the element; $\{\delta U\}$ is the virtual displacement; $\{\delta U_s\}$ is the virtual displacement on the boundary where pressure is prescribed and $\{\delta\overline{U}\}$ is the virtual displacement of boundary nodes where concentrated load is prescribed.

The strains may be related to the nodal displacement by

$$\{\epsilon\} = [B]\{\overline{U}\}, \qquad (20)$$

where $[B]$ is the strain displacement gradient matrix and $\{\overline{U}\}$ is the nodal displacement vector.

The displacements within the elements are related to the nodal displacement by

$$\{U\} = [N]\{\overline{U}\}, \qquad (21)$$

where $[N]$ is the matrix of shape (or interpolation) functions.

Eq. (19) can be reduced to the following matrix form

$$[K_e]\{\overline{U}\} - \{F^{th}\} = \{F\}^b + \{F\}^s + \{\overline{F}\}, \qquad (22)$$

where $[K_e] = \int_\forall [B]^T[D][B]\, d\forall$ is the element stiffness matrix; $\{F^{th}\} = \int_\forall [B]^T[D][\in^{th}]\, d\forall$ is the element thermal load vector; $\{F\}^b = \int_\forall [N]^T[f^B]\, d\forall$ is the elemental body load vector; $\{F\}^s = \int_\eth [N_n]^T[P]\, d\eth$ is the element pressure vector and $[N_n]$ is the matrix of shape functions for normal displacement at the boundary surface.

Assembly of element matrices and vectors of Eq. (22) yields

$$[K]\{\overline{d}\} = \{\overline{R}\},$$

where $[K]$, $\{\overline{d}\}$ and $\{\overline{R}\}$ are the global stiffness matrix, global nodal displacement vector, and global nodal load vector, respectively. Solution of the above set of simultaneous algebraic equations gives unknown nodal displacements and reaction forces. Once the displacement field due to temperature rise in the substrate is known corresponding strain and stresses can be calculated.

The boundary conditions for the stresses imply the followings:

$$\{F^{th}\} = 0, \quad \{F\}^b = 0, \quad \{F\}^s = 0.$$

Table 2
Pulse properties used in the simulation

Pulse intensity (W/m^2)	Heating period (ns)	f
0.5×10^{11}	0.06–0.6	10^{-4}

Gold is used as the workpiece material. The thermophysical properties of gold are given in Table 1 while the step input pulse intensity and the f value used in the computations are given in Table 2.

4. Results and discussions

The thermal stresses developed due to short pulse laser heating of gold were simulated. Since the temperature response of the substrate material was given in a previous study [16], only the three-dimensional stress field including the thermomechanical coupling effect is presented here. The resulting stress field is axisymmetric. Consequently, the stress distribution in the transverse direction (y-axis) is identical to that corresponding to the z-axis stress for a given depth in the substrate. Therefore, the stress distribution in the x–y plane is presented.

Fig. 1 shows the transverse stress component distribution along the y-axis at different locations in the x-axis and $z = 0$ for two heating periods. The stress is compressive in the surface vicinity. As the axial distance from the surface increases, the stress becomes tensile. The magnitude of the stress is very high in the surface vicinity and it reduces rapidly as the location in the x-axis increases from the surface. In the early heating period (0.06 ns), the stress component reduces as distance along the y-axis increases. In this case, the stress component in the surface vicinity ($x = 10^{-8}$ m) reduces at a slow rate in the transverse direction away from the irradiated spot center ($0 \leqslant y \leqslant 0.2 \times 10^{-4}$ m) and this decay rate accelerates along $0.2 \times 10^{-4} \leqslant y \leqslant 7 \times 10^{-4}$ m. This occurs due to the temperature distribution in the surface vicinity of the substrate material across the irradiated spot center, i.e., the temperature decays in the transverse direction across the irradiated spot because of the spatial distribution of the power intensity, which is Gaussian (Fig. 2) [16]. In the case of a long heating period (0.6 ns, Fig. 1(b)) the stress component shows similar behavior to that shown in Fig. 1(a). However, the stress along the transverse direction reduces to almost zero at $x = 2.5 \times 10^{-7}$ m below the surface. As the depth increases beyond $x = 4.5 \times 10^{-7}$ m, the stress component becomes compressive, provided that the magnitude of the stress level reduces.

Fig. 3 shows the axial stress component along the x-axis at different y-axis locations and $z = 0$ for two heating periods. In the early heating period (0.06 ns, Fig. 3(a)), the axial stress component is compressive for $x \leqslant 2 \times 10^{-7}$ m and $y > 5.25 \times 10^{-4}$ m. The opposite is true for $x \leqslant 2 \times 10^{-7}$ m and $y \leqslant 5.25 \times 10^{-4}$ m. Moreover, the magnitude of the stress attains high values close to the surface and it reduces to zero at some depth below the surface. This is because of the temperature field; in this case the lattice site temperatures attain low values and their time derivatives also become low as the distance from the surface increases towards the bulk of the substrate material (Fig. 4). In the case of a relatively long heating period (0.6 ns, Fig. 3(b)), the axial stress component behaves similar to those shown in Fig. 3(a), provided that the stress level increases. The values of stress component reduces close to the irradiated spot center ($y = 1.5 \times 10^{-4}$ m).

Fig. 5 shows the three-dimensional view of the von Mises stresses developed in the substrate material at two heating periods while Fig. 6 shows the variation of von Mises stress along the x-axis at different y-axis locations for two heating periods. In the early heating period (0.06 ns, Fig. 6(a)), the von Mises stress attains relatively high values in the surface vicinity and it reduces as the distance from the surface increases. Moreover, the stress reduces to almost zero at about $x = 2.2 \times 10^{-7}$ m below the surface and it increases gradually with increasing

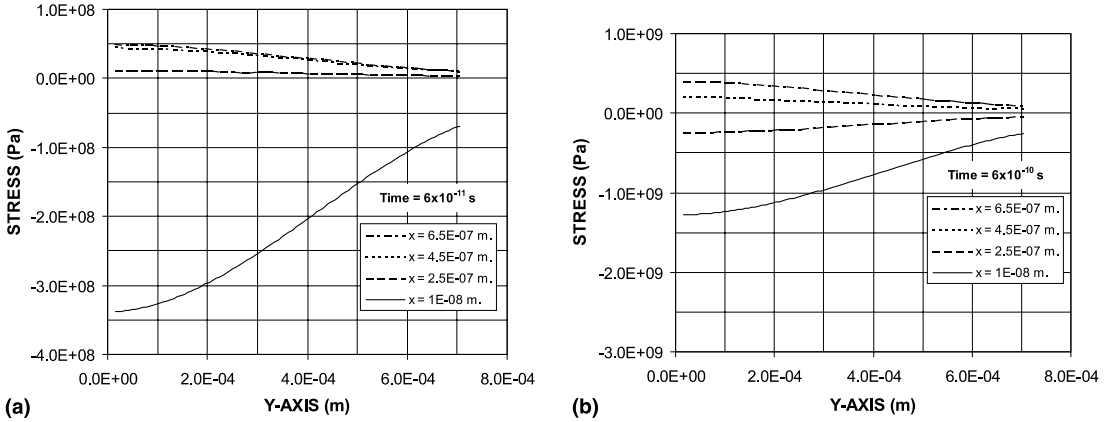

Fig. 1. (a) Stress component in transverse direction along the y-axis at 0.06 ns heating period. (b) Stress component in transverse direction along the y-axis at 0.6 ns heating period.

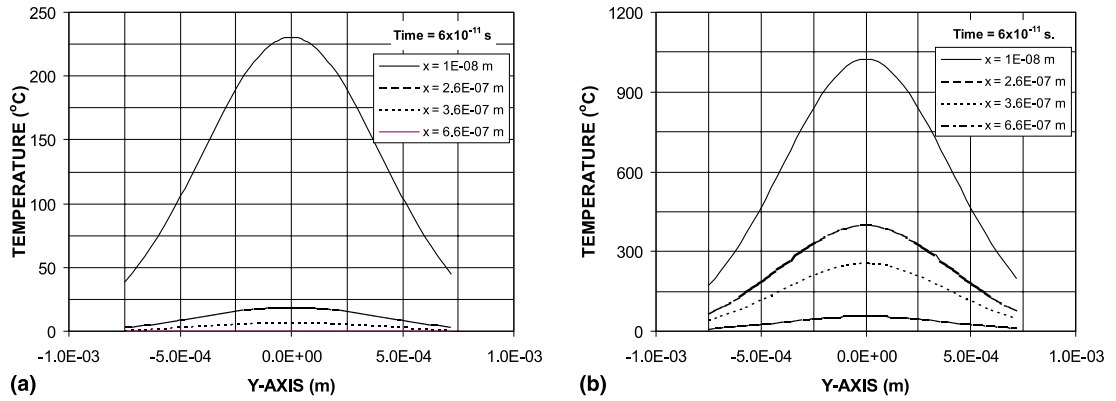

Fig. 2. Temperature profiles along the y-axis at two heating periods. (a) Temperature profiles along the y-axis at heating period of 0.06 ns. (b) Temperature profiles along the y-axis at heating period of 0.6 ns.

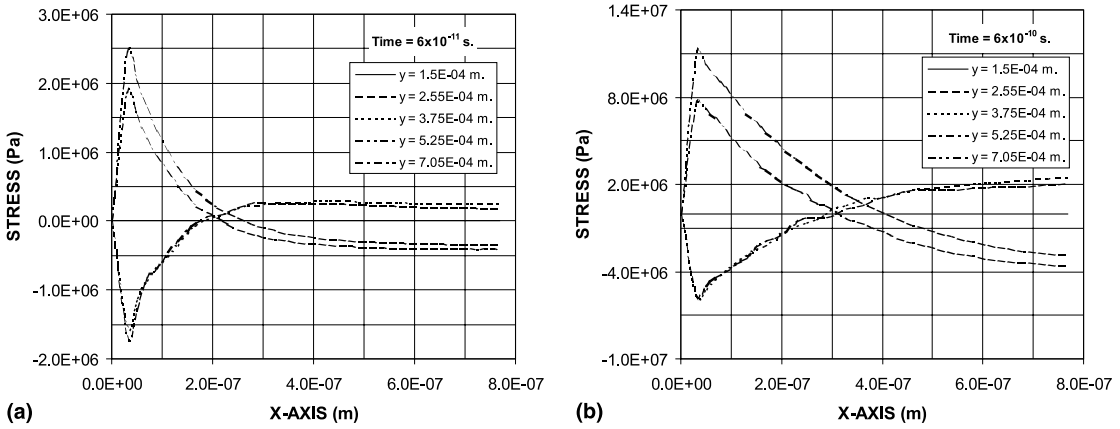

Fig. 3. (a) Stress component in axial direction along the x-axis at 0.06 ns heating period. (b) Stress component in axial direction along the x-axis at 0.6 ns heating period.

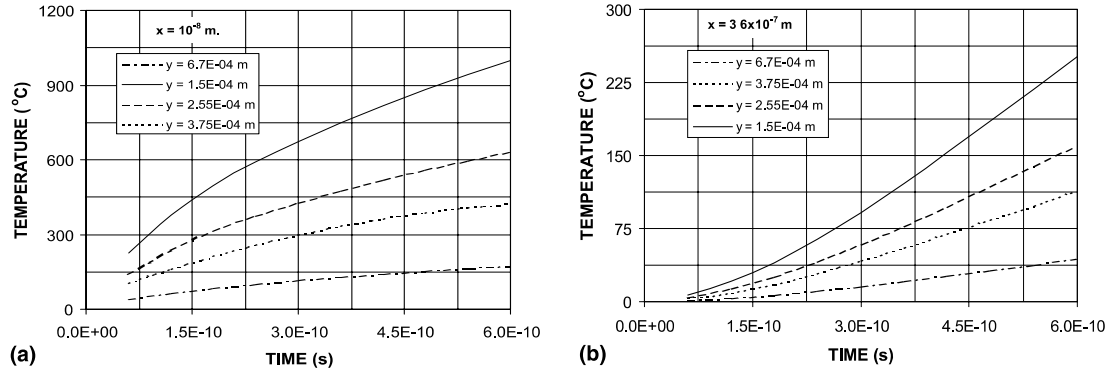

Fig. 4. Temporal variation of temperature profiles at different x, y-axes locations. (a) Temporal variation of temperature profiles at $x = 1E{-}08$ m and different y-axis locations. (b) Temporal variation of temperature profiles at $x = 3.6E{-}08$ m and different y-axis locations.

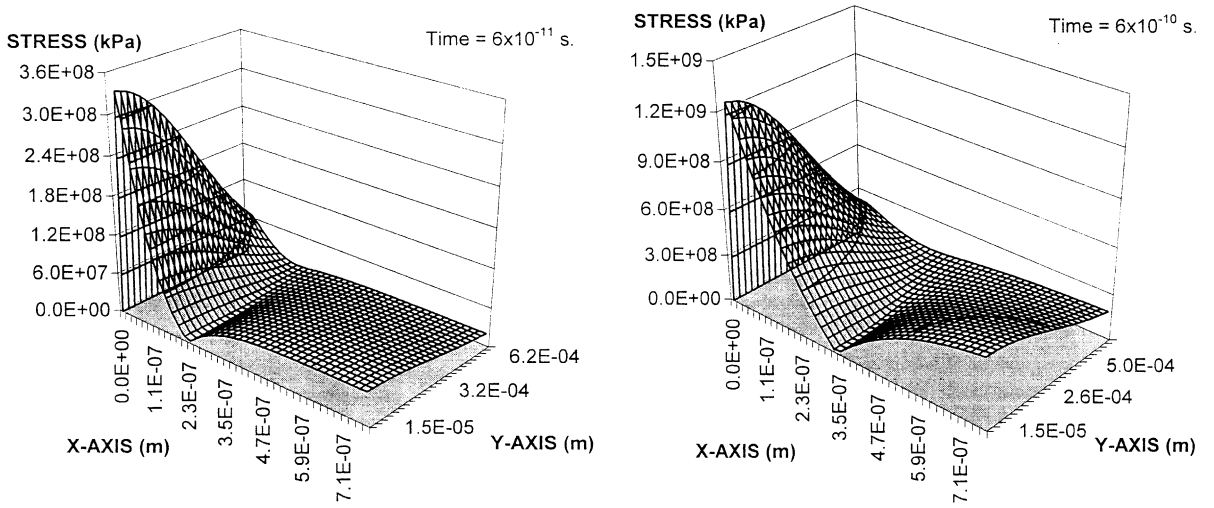

Fig. 5. Dimensional plot of von Mises stresses at different heating periods.

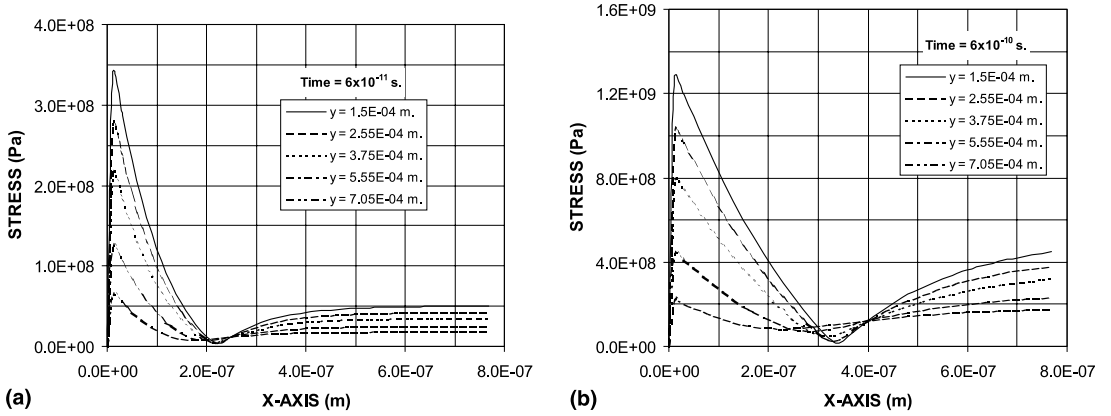

Fig. 6. (a) von Mises stress along the x-axis at 0.06 ns heating period. (b) von Mises stress along the x-axis at 0.6 ns heating period.

axial distance from the point of minimum stress. This behavior is because the transverse stress component, which has a higher magnitude as compared to the axial stress component. In the case of long heating duration (0.6 ns, Fig. 6(b)), the von Mises stress attains relatively higher values than those presented in Fig. 7(a). The location of minimum stress moves further away from the substrate along the x-axis as compared to its counterpart obtained at low heating period, i.e., the location of minimum stress is $x = 2.2 \times 10^{-7}$ m below the surface for 6×10^{-11} s heating period, but it is $x = 3.5 \times 10^{-7}$ m below the surface for the 6×10^{-10} s heating period. This is because the temperature in the surface vicinity, which increases rapidly as the heating progresses (Fig. 4). It should be noted that in the early heating period (0.06 ns), the non-equilibrium heating governs the energy transport in the surface vicinity. However, at 0.6 ns heating period, the equilibrium heating initiates, which enhances the diffusional energy transport in the surface vicinity as indicated in the previous study [16]. Consequently, the material response to a short heating pulse changes as the heating progresses, which in turn results in different stress levels in the substrate. The high stress levels in the surface vicinity are because the temperature rise in the surface vicinity along the transverse direction. In this case, the temperature rises rapidly in the surface vicinity due to the collisional process (Fig. 4). Moreover, the surface is not irradiated uniformly across the transverse direction due to the laser power intensity distribution across the irradiated spot. Consequently, the stress corresponding to $y = 6.5 \times 10^{-4}$ m does not result in considerable stress levels in the axial directions.

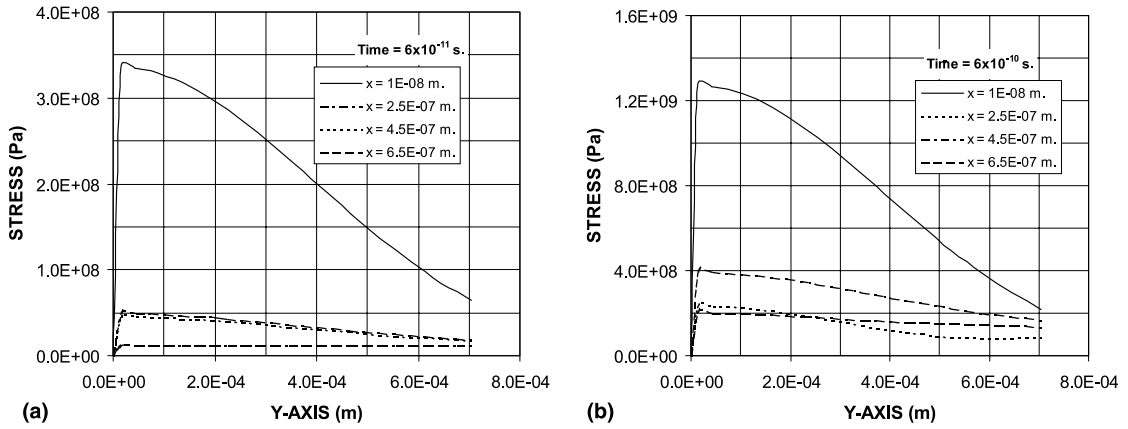

Fig. 7. (a) von Mises stress along the y-axis at 0.06 ns heating period. (b) von Mises stress along the y-axis at 0.6 ns heating period.

Fig. 7 shows the von Mises stress along the transverse direction at different axial locations for two heating periods. In the early heating period (0.06 ns, Fig. 7(a)), the von Mises stress along the transverse direction and close to the surface attains considerably larger values as compared to that of other axial locations. This is because of the temperature distribution in the axial direction; in this case, a temperature gradient on the order of 10^{-8} K/m occurs in the surface vicinity [16]. In the case of long heating period (0.6 ns, Fig. 7(b)), the von Mises stress shows similar behavior to that obtained for early heating period (0.06 ns) in the surface vicinity. However, as the axial distance increases from the surface, the stress attains higher values as compared to that corresponding to the early heating period at the same axial location. This is because of the temperature profile in the substrate; in this case, the lattice site temperature increases in the surface vicinity as the heating progresses (Fig. 4) [16]. As the depth in the axial direction increases to 4.9×10^{-7} m, the stress reduces and it does not vary along the transverse direction.

Fig. 8 shows the temporal variation of von Mises stress at different axial and radial locations. The discussions for the results are given due to the stress levels at different axial locations.

The location of $x = 10^{-8}$ m *below the surface* (*Fig.* 8(a)): The von Mises stress attains the highest value for all locations in the transverse direction. The rise of the stress is higher in the early heating period and it reduces as the heating progresses. This behavior is similar to that corresponding to the temperature (Fig. 4). The reduction in stress level at different locations in the transverse direction is due to the power intensity distribution across the irradiated spot, i.e., it is Gaussian, which in turn results in a decreasing temperature close to the edge of the irradiated spot center.

The location of $x = 2.5 \times 10^{-7}$ m *below the surface* (*Fig.* 8(b)): The von Mises stress shows a different trend as compared to that of $x = 10^{-8}$ m below the surface. The stress in the region away from the irradiated spot center ($y = 2.5 \times 10^{-4}$ m) reduces in the early heating period. It, then, increases rapidly as the heating progresses. This indicates that in the region away from the irradiated spot center, the stress attains the minimum in the early heating period and the point of minimum stress moves away from the irradiated spot center as the heating progresses. Moreover, the stress variation with time is almost linear beyond the point of minimum stress.

The locations of $x = 4.5 \times 10^{-7}$ m *and* $x = 6.5 \times 10^{-7}$ m *below the surface* (*Figs.* 8(c) and (d)): The von Mises stress increases in the early heating period and the rate of increase reduces as the heating time progresses. As the distance moves close to the irradiated spot center, the rate of increase in stress remains almost the same, i.e., as the location in the transverse direction increases further close to the irradiated spot center, the stress increases steadily with time. It should be noted that the rise of temperature at $x = 4.5 \times 10^{-7}$ m slows due to the fact that (i) the absorption depth is less than 4.5×10^{-7} m; therefore, no laser energy is absorbed in this region, and (ii) the temperature rise in this region is because of the heat diffusion, which is not substantiated at low heating period [16]. The magnitude of stress is lower at $x = 4.5 \times 10^{-7}$ m than that of at $x = 6.5 \times 10^{-7}$ m (Fig. 8(d)). This indicates that the compression and tensile stress levels attain the minimum at this depth below the surface. However, the stress increases steadily with time at $x = 6.5 \times 10^{-7}$ m.

Fig. 9 shows the high order terms $((\partial/\partial t)(\nabla \cdot U)$ and $(\partial/\partial t)(\nabla^2 \cdot T))$ in the energy transport equation (Eq. (10)). The values of $(\partial/\partial t)(\nabla^2 \cdot T)$ are larger than the values of $(\partial/\partial t)(\nabla \cdot U)$. This may suggests that the high order term due to temperature rise influences the energy transport more than its counterpart due to displacement. Consequently, the effect of thermomechanical

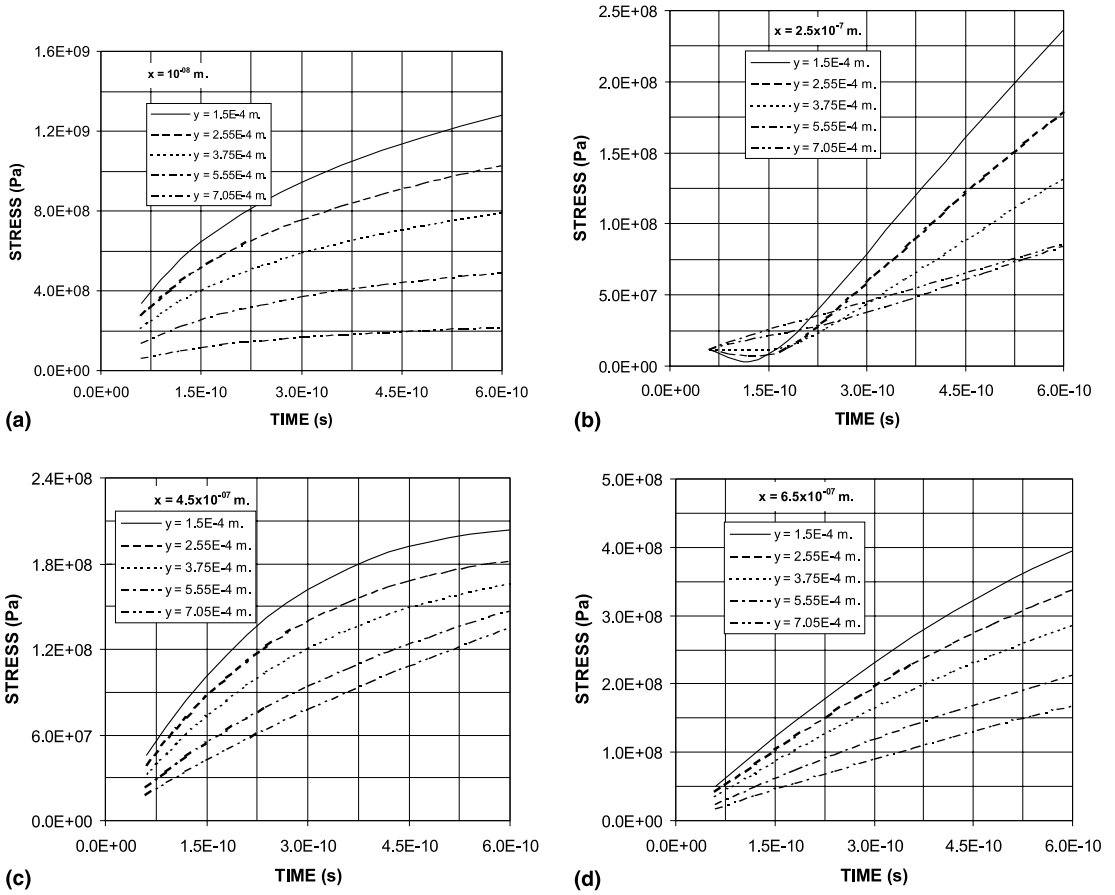

Fig. 8. (a) Temporal variation of von Mises stress $x = 10^{-8}$ m. (b) Temporal variation of von Mises stress $x = 2.57 \times 10^{-8}$ m. (c) Temporal variation of von Mises stress $x = 3.75 \times 10^{-8}$ m. (d) Temporal variation of von Mises stress $x = 6.75 \times 10^{-8}$ m.

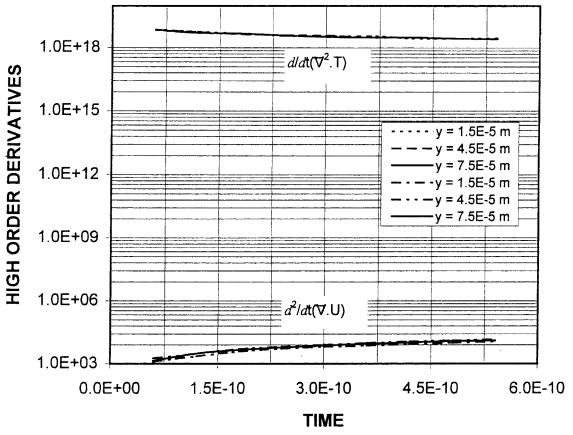

Fig. 9. Temporal variation of the logarithmic values of high order differential terms in the energy transport equation.

coupling on the energy transport is considerably small for the heating conditions considered in the present study. This is because of the low lattice site temperature (~200°C) as well as small displacement of the surface, which is on the order of 10^{-9} m.

5. Conclusions

The thermo-elastic response of gold due to sub-nanosecond (0.06–0.6 ns) laser pulse heating is considered, and the stress field and von Mises stress are predicted. In general, it is found that the stress field does not follow the temperature field in the substrate material. The temporal behavior of von Mises stress differs considerably at different depths below the surface. Moreover, a stress level on the order of 10^9 Pa occurs in the surface vicinity of the substrate material. The specific conclusions derived from the present study are listed as follows:

1. The stress in the transverse direction is compressive in the surface vicinity of the substrate. As the distance from the surface increases along the x-axis, the transverse stress component reduces rapidly. The stress

component also varies along the irradiated region along the y-axis, such that the decay rate of the stress component increases along 0.2×10^{-4} m $\leqslant y \leqslant 4.5 \times 10^{-4}$ m. Moreover, as the heating progresses, the stress component reduces to almost zero at $x = 2.5 \times 10^{-7}$ m below the surface and it becomes compressive at depths below this point.

2. The axial stress component is tensile in the surface vicinity of the substrate for $y < 5.25 \times 10^{-4}$ m. As the distance from the surface increases further this reverses. The magnitude of the stress component does not vary considerably at different locations in the substrate. At the long heating period, the stress component behaves similar to that corresponding to the early heating period, provided that the stress level increases at the long heating period.
3. The von Mises stress attains high values in the surface vicinity and it reduces along the transverse direction. In the case of a long heating period (0.6 ns), the magnitude of the stress increases; however, as the axial depth from the surface increases beyond $x = 4.5 \times 10^{-7}$ m the magnitude of stress reduces considerably to small values.
4. The temporal behavior of the von Mises stress varies considerably at different locations in the substrate. The stress level increases rapidly with time in the region close to the substrate surface. As the heating progresses, the stress rises steadily. Moreover, as the depth from the surface increases, the stress increases slightly with heating time provided that the magnitude of the stress is less. Although the temperature reduces with depth below the surface, the temperature gradient is large. Consequently, the large temperature gradient generates high stress levels in the substrate material.

Acknowledgements

The authors acknowledge the support of King Fahd University of Petroleum and Minerals, Dhahran, Saudi Arabia, for this work.

References

[1] B.S. Yilbas, S.Z. Shuja, Laser short-pulse heating of surfaces, J. Phys. D: Appl. Phys. 32 (1999) 1947–1954.
[2] B.S. Yilbas, The validity of Fourier theory of radiation heating of metals, Res. Mechanica 24 (1988) 377–382.
[3] R.E. Harrington, Application of the theory of heat conduction to the absorption of blackbody radiation, J. Appl. Phys. 38 (1967) 3266–3271.
[4] J.G. Fujimoto, J.M. Liu, E.P. Ippen, Femtosecond laser interaction with metallic tungsten and nonequilibrium electron and lattice temperatures, Phys. Rev. Lett. 53 (1984) 1837–1840.
[5] H.E. Elsayed-Ali, T.B. Norris, M.A. Pessot, G.A. Mourou, Time-resolved observation of electron–phonon relaxation in copper, Phys. Rev. Lett. 58 (1987) 1212–1215.
[6] T.Q. Qui, C.L. Tien, Femtosecond laser heating of multilayer metals – I. Analysis, Int. J. Heat Mass Transfer 37 (17) (1994) 2789–2797.
[7] L.M. Phinney, C.L. Tien, Electronic desorption of surface species using short-pulse lasers, ASME J. Heat Transfer 120 (1998) 765–771.
[8] M.A. Al-Nimr, V.S. Arpaci, Picosecond thermal pulses in thin metal films, J. Appl. Phys. 85 (1999) 2517–2521.
[9] D.Y. Tzou, A unified field approach for heat conduction from macro-to-micro-scales, ASME J. Heat Transfer 117 (1995) 8–16.
[10] B.S. Yilbas, Heating of metals at a free surface by laser radiation an electron kinetic theory approach, Int. J. Eng. Sci. 24 (8) (1986) 1325–1334.
[11] M.F. Modest, Transient elastic and viscoelastic thermal stresses during laser drilling of ceramics, ASME J. Heat Transfer 120 (1998) 892–898.
[12] K. Li, P. Sheng, Plane stress model for fracture of ceramics during laser cutting, Int. J. Mach. Tools Mfg. 35 (1995) 1493–1506.
[13] Y. Dain, P.D. Kapadia, J.M. Dowden, The distortion gap width and stresses in laser welding of thin elastic plates, J. Phys. D: Appl. Phys. 32 (1999) 168–175.
[14] T. Elperin, G. Rudin, Thermo-elasticity problem for a multilayer coating-substrate assembly irradiated by a laser beam, Int. Commun. Heat Mass Transfer 23 (1996) 133–142.
[15] B.S. Yilbas, M. Sami, S.Z. Shuja, Laser-induced thermal stresses on steel surface, Optics Lasers Eng. 30 (1998) 25–37.
[16] B.S. Yilbas, Electron kinetic theory approach – one- and three-dimensional heating with pulsed laser, Int. J. Heat Mass Transfer 44 (2001) 1925–1936.
[17] B.S. Yilbas, M. Sami, 3-dimensional kinetic theory approach for laser pulse heating, Proc. Inst. Mech. Eng. Part C: J. Mech. Eng. Sci. 213 (1999) 491–506.
[18] M. Sami, B.S. Yilbas, Three-dimensional electron-kinetic theory approach for laser heating: moving heat source consideration, Physica A 256 (1998) 439–462.
[19] D.Y. Tzou, Macro-to-Microscale Heat Transfer, Taylor and Francis, Washington, DC, 1997.
[20] L. Xiao, Numerical Computation of Stress Waves in Solids, Akademie Verlag GmbH, Berlin, 1996.
[21] G.D. Smith, Numerical Solution of Partial Differential Equations: Finite Difference Methods, third ed., Clarendon Press, Oxford, 1985.
[22] K.J. Bathe, Finite Element Procedures, Prentice-Hall, Englewood Cliffs, NJ, 1996, pp. 148–192 (Chapter 6).